M-doped Al$_2$TiO$_5$ (M= Cr, Mn, Co) solid solutions and their use as ceramic pigments

M. Dondi,[b] T. Stoyanova Lyubenova,[c] J.B. Carda[c], M. Ocaña[a]

[a]*Instituto de Ciencia de Materiales de Sevilla (CSIC-UNSE), Americo Vespucio 49, Isla de La Cartuja, 41092 Sevilla, Spain*

[b]*ISTEC-CNR, Istituto di Scienza e Tecnologia dei Materiali Ceramici, Via Granarolo, 64, 48018 Faenza, Italy*

[c]*Universitat Jaume I, Campus del Riu Sec, 12071 Castellon de la Plana, Spain*

Abstract. New ceramic pigments based on the tialite (Al$_2$TiO$_5$) structure, doped with Co (pink), Cr (green) or Mn (brown), were prepared through pyrolysis of aerosols followed by calcination of the obtained powders at 1400°C. The expected decomposition of Al$_2$TiO$_5$ into a mixture of Al$_2$O$_3$ and TiO$_2$ on re-firing was inhibited by Cr-doping and also by co-doping with Mg the Mn or Co doped samples. Microstructure and phase evolution during pigment preparation were monitored by SEM and XRPD. Unit cell parameters of tialite were determined by Rietveld refinement of XRD patterns revealing in all cases the formation of solid solutions where the solubility of dopants in the Al$_2$TiO$_5$ lattice followed the trend: Co < Mn < Cr. Valence state and possible location of dopants in the tialite lattice were investigated by XPS and DRS spectroscopies, which suggested the presence of Cr^{3+} ions in a large interstitial site of the tialite lattice with distorted octahedral geometry, and of Mn^{3+} and Co^{2+} ions at the Al^{3+} octahedral sites of the tialite lattice in the former case, and in both Al^{3+} and Ti^{4+} octahedral sites, in the latter. Technological behaviour of pigments was assessed by testing in ceramic glazes finding that the color stability was reasonably good for the Mn-doped tialite and the Cr-doped pigment although the latter suffered a small loss of green hue, while the Co-doped pigment was not stable in glazes, undergoing a cobalt-leaching effect.

I. Introduction

Ceramic pigments are coloured inorganic compounds with high thermal and chemical stability used to colour ceramic bodies. Many of these materials consist of an oxide matrix doped with transition metal cations which act as chromophore cation. One of the main research activities in this field is the search for new inorganic structures that once doped with proper chromophore ions result in new pigments: cheaper, non toxic or with more attractive shades than those currently used in the ceramic industry.[1-6] Among the suggested candidates is pseudobrookite (Fe$_2$TiO$_5$), whose pigment performance has been recently reported.[7]

Tialite (Al$_2$TiO$_5$) is isomorphous with pseudobrookite. Its orthorhombic structure (space group *Bbmm*, Z=4) contains two different highly distorted octahedral sites, where the Al(III) and Ti(IV) cations are located.[8] It has been shown that these cationic sites can accommodate certain amounts of other metal cations such as Si, Zr and Mg,[9,10] Fe and Cr,[11] and lanthanides,[12] although no attention has been paid to the chromatic properties of the resulting solid solutions since most are not coloured. This compound also presents a high melting point (1860ºC)[13] and an appropriate thermal stability. It must be mentioned that, although pure tialite is well known to decompose on firing at 900-1100ºC, this process can be inhibited by the incorporation of certain metal cations to its crystalline lattice.[11,12] Tialite has also a high mean refractive index (2.07 according to the Gladstone-Dale relationship) making this structure a good candidate for the development of new ceramic pigments.[7, 14]

1

The aim of this paper is to synthesise tialite powders doped with Cr, Co or Mn cations and analyse their thermal, crystallochemical and colour properties in order to explore their potential as ceramic pigments. The synthesis route adopted for this purpose was that based on the pyrolysis of liquid aerosols generated from aqueous solutions of cations precursors, which presents several advantages when compared with the traditional ceramic procedure, such as simplicity, control of particle size distribution and higher reactivity.[15-17] In all cases, the chromophore ion content was varied in order to determine the maximum doping level and to optimize the optical properties of the resulting coloured materials. Finally, different glazes were prepared with the optimum pigments in order to evaluate their behaviour during processing and their performance as ceramic pigments.

II. Experimental

(1) Powder preparation

Aluminium nitrate ($Al(NO_3)_3 \cdot 9H_2O$, Aldrich, >99%), titanium oxychloride ($TiOCl_2 \cdot HCl$, Fluka, Ti content = 15%), magnesium chloride ($MgCl_2 \cdot 6H_2O$, Panreac, 99%), manganese nitrate ($Mn(NO_3)_2 \cdot 4H_2O$, Fluka, 97%) and cobalt nitrate ($Co(NO_3)_2 \cdot 6H_2O$, Aldrich, 98%) were used as metal precursors as received. The powders synthesis was carried out by pyrolysis of liquid aerosols generated from aqueous solutions of these precursors following a procedure previously reported for other pigment systems,[16] which can be summarised as follows. The starting solutions having the tialite stoichiometry (0.1 mol dm^{-3} $Al(NO_3)_3$ and 0.05 mol dm^{-3} $TiOCl_2$, for the samples only doped with Cr, Mn or Co, and 0.09 mol dm^{-3} $Al(NO_3)_3$, 0.005 mol dm^{-3} $MgCl_2$ 0.055 mol dm^{-3} $TiOCl_2$, for the samples containing Mg) and variable concentrations of the chromophore (Table I) were sprayed into an expansion chamber using a glass nozzle and air at constant pressure (0.5 kg cm^{-2}) as a carrier gas. The aerosols so generated flew through two consecutive furnaces kept at 250 and 800ºC, respectively, in which the liquid droplets were dried and thermally decomposed, respectively. The resulting solid particles were finally collected on a glass filter with a very high efficiency.

The as prepared powders were calcined at different temperatures up to 1400ºC for 3 h, placing them in platinum crucible, heating the furnace at 10ºC min^{-1} up to the maximum temperature.

For testing in glazes, aqueous suspensions – containing a 3 wt.% of pigment and a 97 wt.% of a transparent industrial frit (Colores Cerámicos SA, Onda, Castellón, Spain; composition (wt%): Al_2O_3 <10%, B_2O_3 <5%, CaO <10%, SiO_2 > 60%, Na_2O <10%, ZnO <10%) – were prepared by ball milling. These slurries were deposited on double-firing wall tile bodies and further fired at the 1050ºC using the following thermal schedule: from room temperature to 800ºC with a heating rate of 42ºC min^{-1}, from 800 to 1050ºC at 14ºC min^{-1}, after 5 min at 1050ºC the furnace was switched off and the glazed tiles were left to cool down inside the furnace.

(2) Characterization techniques

The size and morphology of the particles were examined by scanning electron microscopy (SEM) (Model JSM5400, JEOL, Tokyo, Japan). Energy dispersive X-ray analysis (EDX) (Oxford, Model Link) installed in the scanning electron microscope was used to gain information on the particles composition.

The crystalline phases present in the solids were identified by X-ray diffraction (XRD) (Model D501, Siemens, Karlsruhe, Germany). Unit cell parameters were determined by a least squares refinement from the X-ray diffraction data collected at intervals of 0.02° (2θ) for an accumulation time for interval of 10 s, using silicon (20% by weight) as internal

standard. The crystallographic data for the Al_2TiO_5 structure were taken from the JCPDF file reported for this compound (JCPDS 41-258).

Information on the oxidation state of the chromophore species in the pigments was obtained from the X-ray photoelectron spectra (XPS) of the samples measured with a VG Escalab apparatus (Model 220, West Sussex, UK) using the $AlK\alpha$ excitation source. Calibration of the spectra was done at the Ti2p peak taken at 458.5 eV.

Diffuse reflectance spectroscopy (DRS) was performed by a Perkin Elmer spectrophotometer (Model λ35, Norwalk, CT) under the following conditions: 350-1100 nm range, 0.03 nm step size, $BaSO_4$ integrating sphere, $BaSO_4$ pellet as white reference material. The powders were allocated in sample-holder with quartz glass window. Reflectance (R_∞) was converted to absorbance (K/S) by the Kubelka-Munk equation: $K/S = (1-R_\infty)^2 \cdot (2R_\infty)^{-1}$.[18] Absorbance bands in the 9000-26000 cm^{-1} range were deconvoluted in gaussian peaks (PFM, OriginLab) in order to get energy (centroid), splitting (full width at half maximum, FWHM) and optical density (area). The experimental errors, including background correction and reproducibility, are ~2% (energy), ~5% (splitting) and ~10% (optical density). Every band was attributed by fitting its energy in the relevant Tanabe-Sugano diagrams:[19] (d^3 for Cr^{3+}, d^4 for Mn^{3+}, and d^7 for Co^{2+}). Crystal field strength *10Dq* was determined by the energy of spin-allowed transitions for Cr^{3+} and Co^{2+} [20-22] or by the method of orbital baricentre for Mn^{3+}.[20] Interelectronic repulsion Racah parameters were calculated by energies of spin-allowed bands (B and C Co^{2+}, and B_{35} for Cr^{3+}) or spin-forbidden ones (B_{55} and C for Cr^{3+}).[18,21,22] The attribution of the main bands was verified calculating expected energies on the basis of 10Dq and B values.[18, 21-23] The nephelauxetic ratio β was calculated as $\beta=B/B_0$, where B is experimental and B_0 is the value of the free ion.[18, 21-23]

The color of the pigments was evaluated according to the Commission Internationale de l'Eclairage (CIE) through *L*a*b** parameters.[24] In this system, *L** is the color lightness (L^*=0 for black and L^*=100 for white), *a** is the green (-)/red (+) axis, and *b** is the blue (-)/yellow (+) axis. These parameters were measured (illuminant D65, standard observer 10°) using a Dr. Lange colorimeter (Model LUCI 100, Berlin, Germany) and a white tile ceramic (chromaticity coordinates: x = 0.315, y = 0.335) as standard reference. Before measurements, the samples were gently ground in an agate mortar.

III. Results and discussion

(1) Microstructure and phase evolution during pigment preparation

Table I shows the nominal composition in terms of the chromophore/tialite molar ratio of all samples prepared by the pyrolysis of aerosols procedure, which will be hereafter named as indicated in the table. All samples, irrespective of the chromophore ion, consisted of spherical particles with a broad size distribution (<10 m), as expected from the method here used for aerosol generation.[15-17] An illustrative example of such particles (sample Cr5) is shown in Fig. 1A, in which it can be also observed that they seem to be composed by much smaller subunits strongly aggregated and that some of them were hollow (see the inset of Fig. 1A) indicating the preferential precipitation of the salts precursors near the surface of the aerosol droplets during the drying process in the first furnace.[25]

After spray pyrolysis, all samples were amorphous to XRD; for this reason they were further calcined at increasing temperatures up to the tialite crystallization. As observed in Fig. 2A, which corresponds to sample Cr5, TiO_2 with anatase structure (JCPDS 21-1272) was the first crystalline phase appearing after heating at 800°C. This phase transformed into rutile (JCPDS 21-1276) at 1000°C, which was accompanied by the crystallization of Al_2O_3 corundum (JCPDS 46-1212). The tialite (JCPDS 41-258) crystallization started at 1200°C, ending this process on calcination at 1400°C, although a very small amount of

unreacted corundum still remained in the sample. The thermal behavior of the other Cr-doped samples was similar (data not shown).

In the case of the Mn-doped samples, the only noticeable difference in the crystallization behavior with respect to the Cr-doped system was the occurrence of a very weak and unidentified peak at ~46 °2θ in the XRD diffraction patterns of the samples with a Mn content ≥8% after firing at 1400ºC, whose intensity increased with Mn content (Fig. 2B).

The thermal evolution of the Co-doped samples was also similar to the Cr-doped case, except that for a Co content ≥8%, a small amount of $CoAl_2O_4$ spinel (JCPDS 38-814) was detected by XRD after calcination at 1400ºC, in addition to tialite (Fig. 2C).

In all cases, the thermal treatment gave rise to particle sintering, resulting in irregular grains of similar size in the case of Cr and Co doping (Fig. 1B and C, respectively) and of coarser size (< 15 μm) in the Mn-doped samples (Fig. 1D).

(2) Tialite crystal structure

Table II shows the unit cell parameters determined for all doped-tialite systems calcined at 1400ºC and for an undoped sample obtained by a similar procedure for comparison. As observed, a volume cell expansion was detected in all cases evidencing the formation of M/tialite (M = Cr, Mn or Co) solid solutions. It was also observed that for Cr and Mn doping, the unit cell parameters increased progressively in the whole range of studied compositions (up to a 20% of Cr and 14% of Mn) suggesting that the maximum cation solubility was not attained in these two cases. On the contrary, for the Co-doped samples, these parameters reached a maximum for sample Co8 (Co content = 8%). Since a certain amount of unreacted $CoAl_2O_4$ was detected for this sample (Fig. 2C), it can be concluded that the Co solubility in the tialite lattice is < 8% (Co/tialite mol ratio).

The extent of unit cell expansion depends on the type of dopant (Fig. 3). Tialite exhibits a regular growth of unit cell parameters with increasing amount of Co or Mn doping; exception is made of tialite Co11, which is always out the general trend of Co-doped pigments, confirming that the actual cobalt content in solid solution is lower than the nominal amount. The lattice expansion occurs mainly along the *a* and *b* axes, and it is larger for Co than for Mn doping. In contrast, the Cr-doped tialite lattice undergoes an anisotropic distortion, as it exhibits a smaller expansion mainly along the *c* axis, with little changes of *a* and *b* parameters (Fig. 4).

(3) Valence state of chromophores

To elucidate the chromophore oxidation state in these solid solutions, XPS spectroscopy was used. For this purpose, we selected the samples with the highest doping level below the solubility limit (Cr20, Mn14 and Co5). As observed in Fig. 5, the spectrum of the Cr doped sample displayed two Cr2p peaks at 576.6 ($Cr2p_{3/2}$) and 586.3 ($Cr2p_{1/2}$) eV, which can be attributed to either Cr(III) or Cr(IV) cations, since the binding energy for both cations is very similar.[26,27] However, crystallographic considerations seem to discard the presence of Cr(IV). Thus, if these cations were present, they would most likely occupy the Ti(IV) sites for elecroneutrality. This situation would result in a cell contraction since the ionic radius of Cr(IV) (0.55 Å) is smaller than that of Ti(IV) (0.605 Å),[28] which is in contrast to the unit cell expansion detected for this system (Table II).

The position of the Mn2p XPS peaks of the Mn-doped sample (641.5 and 653. 1 eV, respectively) and the absence in the XPS spectrum of a satellite at about 648 eV characteristic of Mn(II), seem to indicate the only presence of Mn(III) and/or Mn(IV) cations in this sample. These species can not be distinguished by this technique since their binding energy is very close.[29] Again, the unit cell expansion on Mn doping (Table II) and the size of Mn(III) (0.645 Å) and Mn(IV) (0.53 Å) cations[28] drive to discard the existence of

the later because of crystallographic considerations similar to the those above mentioned for the Cr system.

The Co2p XPS spectrum of the Co-doped sample showed two peaks at 780.6 and 796 eV, respectively, along with two satellites at lower binding energy whose relative intensity clearly manifest that only Co(II) species are present in the sample.[30] Therefore, it can be assumed that the solid solution is formed in this system by the simultaneous substitution of two Al(III) for one Co(II) and one Ti(IV) cations to maintain electroneutrality, as it has been previously suggested for other divalent cations/tialite solid solution such as the Mg(II) case.[9] As a consequence, some free alumina would be available for the formation of a cobalt aluminate spinel, which should be also taken into account to explain the small amount of this phase detected in the sample with the higher Co content (8%).

The occurrence of dopants as Co(II), Cr(III), and Mn(III) is in agreement with the observed extent of lattice expansion: Co > Mn > Cr. This trend can be explained by the respective ionic radii in six-fold coordination:[28] Co(II) 0.745 Å, Mn(III) 0.645 Å, and Cr(III) 0.615 Å, which are larger than those of Ti(IV) 0.605 Å and Al(III) 0.535 Å. Interestingly, samples doped with Mg(II) (0.72 Å) follows rather faithfully the above trend with expansion close to that of Co-doped tialite.

(4) Thermal stability of tialite pigments

In order to investigate the thermal stability of the solid solutions formed after calcination at 1400ºC, the same samples used for XPS characterization were further fired for 20 h at 900ºC.[11] The XRD pattern obtained after this treatment for sample Mn14 revealed the complete decomposition of tialite leaving TiO_2 (rutile) and corundum (Al_2O_3), as the main phases (Fig. 6B). Such decomposition was only partial in the case of Co doping (Fig. 6C) whereas it was completely inhibited in the Cr-doped sample whose XRD patterns before (Fig. 2) and after firing (not shown) were very similar. This result is surprising and contrary to previous reports which indicated that Cr-doping has adverse effects on the tialite thermal stability.[11]

In order to improve the thermal stability of these Mn- or Co-doped solid solutions, Mg(II) cations were also incorporated into the tialite lattice since they have been demonstrated to be highly efficient for such a purpose.[9] For this study, we selected the Mn and Co contents resulting in the purest samples according to XRD (sample Mn5 and Co5) and a 10% of Mg (Mg/tialite mol ratio), which involves a tialite stoichiometry given by the formula $Al_{1.8}Ti_{1.1}Mg_{0.1}O_5$ (Table I), to maintain electroneutrality. A sample only doped with Mg was also prepared for comparison. As observed in Fig. 6A, tialite was completely developed in these samples after heating at 1400ºC as in the samples not containing Mg. It is important to note that, for the Co system, a small amount of $CoAl_2O_4$ was also detected by XRD, which was not present in the sample only doped with a similar amount of Co (Fig. 2C) indicating that the presence of Mg reduces the solubility of Co in the tialite lattice. This finding is not surprising considering that Mg(II) and Co(II) are very similar in size and bonding geometry preferences and that the doping level in the Mg-Co codoped sample is much higher (15%) than the solubility limit found for the Co/tialite system (<8%). It should be also mentioned that particle sintering was also detected after calcination in both cases, resulting in particles similar to those of the samples only doped with Mn or Co (Fig. 1C and 1D). The formation of solid solutions in the Mg-doped samples is corroborated by the increase of their unit cell parameters when compared with those of the undoped sample as the amount of dopants increased (Table II, Fig. 3). The presence of Mg(II) cations in these solid solutions seems that to have little or no influence on the Mn or Co oxidation state, since the XPS spectra of the samples containing Mg are very similar to those of Mg-free samples (Fig. 5). Finally, the effectiveness of Mg doping for the stabilization of the Mn- or Co-doped tialite solid solutions was evidenced by the XRD patterns obtained in both cases

after a further firing at 900ºC for 20 h, which point out that tialite is the main crystalline phase (Fig. 6B ad C).

(5) Colour

The *L*a*b** parameters and color of all synthesized tialite solid solutions are shown in Table III. As observed, Cr doping results in green pigments with very similar hue (a* and *b** values) irrespective of the doping level. The amount of dopant only affected in a significant manner the value of lightness (*L**) which decreased (darker color) as increasing the Cr content. From these parameters it can be also concluded that the optimum pigment (best color with the lower doping level) was that containing a 14% of Cr since the increase of this value up to 20% did not yield an important increase of *L**. All the Mn-doped pigments showed a brown color whose intensity increased (*L** decreased) as increasing the Mn content up to a 11%, remaining almost constant for higher doping levels. The increase of the Mn amount also resulted in a progressive shift to more achromatic shades (*a** and *b** decrease). More appreciable color changes were detected for the Co-doped pigments when the amount of Co was varied. Thus, the more diluted sample (Co content = 5%) showed a pale salmon pink color which shifted to a beige hue when the Co content was increased up to 8% (sample Co). A further increase of the later amount up to 11% (sample Co11) resulted in a darker and more achromatic (lower *a** and *b**) shade. These color changes were probably due to the presence of a certain amount of $CoAl_2O_4$ in addition to the Co-tialite solid solution in samples Co8 and Co11, which was higher in the later pigment, as detected by XRD (Fig. 2C). Therefore, the most interesting Co-doped pigment is that with a Co content of 5% (Sample Co5).

The *L*a*b** parameters of the Mg,Mn-codoped tialite pigment (Sample MgMn5) were similar to those of the sample only doped with a similar amount of Mn (sample Mn5) and therefore, showed a similar brown hue (Table III). However, the addition of Mg to the Co-tialite solid solution (sample MgCo5) resulted in a shift from pale salmon pink to darker (lower *L**) and more achromatic dun color (Table III) likely due to the presence in this sample of the excess of $CoAl_2O_4$ detected by XRD (Fig. 6A).

(6) Optical spectroscopy

The UV-visible-NIR spectrum of the optimum Cr-doped tialite pigment (sample Cr14) exhibits the expected bands of Cr(III) in octahedral coordination (Fig. 7A): the intense spin-allowed transitions $^4T_{2g}$ and $^4T_{1g}$ as well as the weak spin-forbidden transitions ^2E_g, $^2T_{1g}$ and 2T2g.[20-23] However, the spectrum also presents some unusual features, as the strong absorbance at the visible-UV border and the band at about 11500 cm^{-1}. The former, which is not referable to any Cr-O or Al-O charge transfer,[21] is perhaps due to a Ti-O metal-ligand charge transfer, as it occurs in titania.[31-32] The latter is not ascribable to any Cr(III) transition. The resulting optical parameters of six-fold coordinated Cr(III) are: crystal field strength Dq=1520 cm^{-1}, Racah B_{35}=690 cm^{-1}, B_{55}=618 cm^{-1} and C=2873 cm^{-1}; these values correspond well with calculated energies of Cr(III) bands (Table IV). However, the crystal field Dq is not consistent with the metal-oxygen bond distance, since in Al_2TiO_5 the mean Al-O distance is 1.94 Å, the expected Dq should be around 1750 cm^{-1}, according to the main trend of oxides and silicates.[20] A Dq as low as 1520 cm^{-1} matches a large crystallographic site, having a metal-oxygen distance of at least 2 Å (Fig. 7B). In any case, there are crystal structures which do not strictly follow the crystal field theory model, because the Cr(III) is at interstitial sites, e.g. mullite,[33] or in strongly distorted sites, e.g. zoisite.[34] Interestingly, the spin-allowed bands of Cr14 are very broad, almost at the limit for crystal field transitions (e.g. FWHM over 4000 cm^{-1}); this may imply a strong local distortion of the CrO_6 site. A possible interstitial site in the tialite lattice is present along

6

"channels" parallel to the *b* axis, where a strongly distorted octahedral site is envisaged with a mean M-O distance around 2 Å.[35]

The spectra of all Mn-doped samples (even that co-doped with Mg) were similar each other and exhibit a strong absorbance of the green-blue-violet light and another absorbance peak in the near infrared; the main difference is absorbance, which clearly increased with manganese content from Mn5 to Mn14 and slightly diminished with Mg co-doping (Fig. 8A). There are clues of at least four main bands peaking at about 11000, 16000, 19000 and 22000 cm^{-1}, respectively; however, the deconvolution requires two further bands at about 10000 and 25000 cm^{-1} (Fig. 8B). These features may be attributed to Mn(III), in agreement with XPS results and the crystallographic considerations above discussed, which typically undergoes Jahn-Teller effect with a strong splitting of the energy of orbitals e_g and t_{2g}.[20,21] From this standpoint, the splitting of the lowest energy field state is thought to be responsible for the peak at ~11000 cm^{-1}, while double splitting of the t_{2g} orbitals may be claimed for the bands at higher energy. At all events, this simple interpretation is able to explain just the main optical features: one band in the infrared and the two intense bands at approximately 19000 and 22000 cm^{-1}; the apparent doubling of bands, involving those at ~16000 and 25000 cm^{-1}, might be due to distinct contributions from the two slightly different octahedral sites or to the unidentified phase (Fig. 2B). According to this interpretation, the crystal field strength is estimated to be on average Dq=1530 cm^{-1} (Table V). This value is in fair agreement with the relationship between Dq and Mn(III)-O distance in known structures. For instance, tialite presents values of Dq and Mn-O distance close to those of andalusite, where Mn(III) occupies a very distorted octahedral site of aluminium (average Al-O distance 1.94 Å).[20,36]

The spectra of samples Co5 and MgCo5 are significantly different, even by a fingerprinting approach (Fig. 9). It appears that the sample only doped with Co (Co5) has mostly Co(II) in sixfold coordination since its spectrum is similar to that of Co-olivine (Fig. 9A), which has only Co(II) in octahedral coordination,[7,38] while the sample co-doped with Mg and Co (MgCo5) contains essentially Co(II) in tetrahedral coordination. In fact, the energies of the main bands of the latter sample correspond to those of Co-doped willemite (Fig. 9A), which has only fourfold-coordinated Co^{2+}.[39-40] The spectrum of sample Co5 has been interpreted deconvolving 5 bands, attributed to three spin-allowed transitions: $^4T_{1g}$ (^4F) → $^4T_{2g}$, $^4A_{2g}$, $^4T_{1g}$ (^4P); and two spin-forbidden ones: $^4T_{1g}$ (^4F) → $^2T_{2g}$ and $^2A_{1g}$ (Fig. 9B). The broad absorbance at the UV-visible border is likely to be due to Ti-O charge transfer. These bands fit the Tanabe-Sugano diagram for a crystal field strength Dq=946 cm^{-1} and a Racah B=760 cm^{-1} (C=4B=3040 cm^{-1}); these values reasonably match with calculated energies of Co(II) bands (Table IV). In the literature, there are too few data of crystal field strength of Co(II) to allow a reliable relationship with crystal structure and infer Co-O distance. The bands corresponding to tetrahedral Co(II) in the spectrum of sample MgCo5 must be attributed to the presence of the above mentioned small amount of $CoAl_2O_4$ spinel detected by XRD (Fig. 6A).

(7) Technological behavior

The industrial applicability of the colored tialite-based systems was assessed by choosing the optimum Cr pigment (sample Cr14) and the Mn and Co pigments with the doping levels which gave rise to the purest tialite (samples Mn5, Co5, MgMn5 and MgCo5). In all cases, glazes free of defects were obtained as illustrated in figure 10 for samples Cr14, Mn5 and Co5, although some appreciable differences in color with respect to that of the powdered samples were detected (Table III). Thus, a darker (lower *L**) green shade was observed for the Cr-doped pigment, which also showed a higher value of *a** (less green) and *b** (more yellow) components. In the case of Mn-doping, a lighter (higher *L**) and more orange (higher *a** and *b**) brown color was observed after glaze firing. Similar

parameters and tendency were observed for the tiles decorated with the Mg,Mn co-doped pigment. This similarity suggests that the Mn-tialite solid solution was not affected during the thermal treatment used in glaze test, even in the absence of Mg, probably due to the short holding time at high temperature. The most significant hue shift induced by application in glaze was observed for the Co-doped pigment, which changed from pale salmon pink to grey probably as a consequence of the exsolution of the Co cations from the tialite lattice during this process (the so-called *cobalt leaching*[38, 41]). This interpretation may be supported by the similar grey color obtained for the glaze prepared with the Mg,Co-codoped pigment (Table III), which already presented an excess of $CoAl_2O_4$ before enameling (Fig. 6A).

IV. Conclusions

New ceramic pigments with the tialite structure doped with Cr, Mn or Co cations were for the first time obtained by pyrolysis of aerosols followed by a further calcination of the obtained powders at 1400 °C. In all cases, tialite solid solutions were achieved, but at high doping levels for Co and Mn, spinel-like secondary phases were also present. The solubility of dopants in the Al_2TiO_5 lattice is growing in the series: Co < Mn < Cr. The expected decomposition of Al_2TiO_5 into Al_2O_3+TiO_2 on re-firing over 900°C was inhibited in the Cr-doped pigments and it was also prevented by co-doping with Mg^{2+} cations the Co or Mn doped tialite solid solutions. Spectroscopic data indicate that Mn^{3+} and Co^{2+} ions are accommodated at the octahedral sites of the tialite lattice, mainly substituting for Al^{3+} in the former case and for both, Al^{3+} and Ti^{4+} ions, in the latter, implying an expansion of the unit cell, mostly along the *a* and *b* axes, proportional to the difference in ionic radii. Cr^{3+} seems to rest in a large interstitial site, with distorted octahedral geometry, implying an anisotropic lattice expansion mainly along the *c* axis. The colours achieved are green, brown and pink, as expected in the case of Cr^{3+}, Mn^{3+} and Co^{2+} in octahedral coordination, respectively. The colour stability after application in ceramic glaze is satisfactory for the Mn-doped tialite and the Cr-doped pigment although the latter suffers a small loss of green hue, perhaps related to the peculiar location of chromium ions in the Al_2TiO_5 structure. The Co-doped pigment is not stable in the glaze, as it underwent a typical cobalt-leaching effect, with diffusion of Co ions into the glassy phase.

References

[1] M. Trojan, P. Sulcova, P. Mosner, "The synthesis of binary zinc(II)-nickel(II) cyclo-tetraphospahtes as new special pigments", *Dyes and Pigments* **44**, 161-4 (2000)

[2] R. Ricceri, S. Ardizzone, G. Baldi, P. Matteazzi, "Ceramic pigments obtained by sol-gel techniques and by mechanochemical insertion of color centers in Al_2O_3 host matrix", *Journal of the European Ceramic Society*, **22**, 629-37 (2002)

[3] E. Lopez-Navarrete, V.M. Orera, F.J. Lazaro, J.B. Carda, M. Ocaña, "Preparation through aerosols of Cr-doped $Y_2Sn_2O_7$ (pyrochlore) red-shade pigments and determination of the Cr oxidation state", *Journal of the American Ceramic Society* **87**, 2108–13 (2004)

[4] R. Galindo R, M. Llusar, M.A. Tena, G. Monros, J.A. Badenes, "New pink ceramic pigment based on chromium(IV)-doped lutetium gallium garnet", *Journal of the European Ceramic Society* **27**, 199-205 (2007)

[5] M. Martos, B. Julian-Lopez, E. Cordoncillo and P. Escribano, "Structural and spectroscopic study of a novel erbium titanate pink pigment prepared by sol-gel methodology", Journal of Physical Chemistry B, **112,** 2319-25 (2008)

[6]M. Dondi M, F. Matteucci, G. Baldi, A. Barzanti, G. Cruciani, I. Zama, C.L. Bianchi, "Gray-blue Al_2O_3-MoO_x ceramic pigments: Crystal structure, colouring mechanism and performance", *Dyes and Pigments*, **76**, 179-86 (2008)

[7]M. Dondi, F. Matteucci, G. Cruciani, G. Gasparotto, D.M. Tobaldi, "Pseudobrookite ceramic pigments: Crystal structural, optical and technological properties", *Solid State Sciences* **9**, 362-369 (2007)

[8]B. Morosin B, R.W. Lynch, "Structure studies on Al_2TiO_5 at room temperature and at 600ºC", *Acta Crystallographica* **B28,** 1040-1046 (1972)

[9]M. Ishitsuka, T. Sato, T. Endo, M. Shimada,"Synthesis and thermal stability of Aluminium Titanate solid solutions", *Journal of the American Ceramic Society* **70,** 69-71 (1987)

[10]L. Giordano, M. Viviani, G. Bottino, M. T. Buscaglia. V. Buscaglia, P. Nanni, "Microstructure and thermal expansion of Al_2TiO_5- $Mg_2Ti_2O_5$ solid solutions obtained by reaction sintering", *Journal of the European Ceramic Society*, **22,** 1811-22 (2002)

[11]T.L. Lekanova, Y.I. Ryabkov, A. Sevbo, V.V. Viktorov, "Phase relations in the systems Al_2TiO_5-Fe_2O_3, Al_2O_3-TiO_2-Fe_2O_3, and Al_2TiO_5-Cr_2O_3", *Inorganic Materials* **40,**1355-9 (2004)

[12]S. Djambazov, D. Lepkova, I. Ivanov, "A study of the stabilization of aluminium titanate", *Journal of Materials Science* **29,** 2521-5 (1994)

[13]A. Tsetsekou, "A comparison study of tialite ceramics doped with various oxide materials and tialite-mullite composites: microstructural, thermal and mechanical properties", *Journal of the European Ceramic Society* **25**, 335-48 (2005)

[14]F. Matteucci, G. Cruciani, M. Dondi, G. Gasparotto, D. M. Tobaldi, "Crystal structure, optical properties and colouring performance of karrooite $MgTi_2O_5$ ceramic pigments", *Journal of Solid State Chemistry* **180**, 3196-210 (2007)

[15]P. Tartaj, T. Gonzalez-Carreño, C. J. Serna, M. Ocaña, "Iron zircon pigments prepared by pyrolysis of aerosols", *Journal of Solid State Chemistry,* **128**, 102–8 (1997)

[16]E. Lopez-Navarrete, M. Ocaña, "A simple procedure for the preparation of Cr-doped tin sphene pigments in the absence of fluxes", *Journal of the European Ceramic Society*, **22**, 353–9 (2002)

[17]E. Lopez-Navarrete, A. Caballero, A.R. Gonzalez-Elipe, M. Ocaña, "Low temperature preparation and structural characterization of Pr-doped ceria solid solutions", *Journal of Materials Research,* **17,** 797-804 (2002)

[18]S. Marfunin, "Physics of minerals and inorganic materials. An introduction"; p 340, Springer-Verlag, Berlin, 1979

[19]Y. Tanabe, S. Sugano, "On the absorption spectra of complex ions, I, II"; *Journal of Physical Society of Japan*, **9**, 753-766, 767-779 (1954)

[20]R. G. Burns R.G, "Mineralogical applications of crystal field theory, 2nd ed.", p 551, Cambridge University Press, New York, 1993

[21]B. P. Lever, "Inorganic electronic spectroscopy, 2nd ed."; p 863, Elsevier, Amsterdam, 1984

[22]M. Wildner M, M. Andrut, C. Z. Rudowicz, "Spectroscopic methods in mineralogy"; pp 93-144, Vol. 6, Edited by A. Beran and E. Libowitzky", Eötvös University Press, Budapest, 2004

[23]M. Andrut M, M. Wildner, C. Z. Rudowicz, "Spectroscopic methods in mineralogy", pp 145–188, Vol. 6, Edited by A. Beran; E. Libowitzky, Eötvös University Press, Budapest, 2004

[24]Commission Internationale de l'Eclairage, "Recommendations on uniform colour spaces, colour difference equations, psychometrics colour terms", Supplement no. 2 of CIE publication no.15 (E1-1,31) 1971, Paris, Bureau Central de la CIE, 1978

[25]G. L. Messing, S. C. Zhang, G. V. Jayanthi, "Ceramic powder synthesis by spray pyrolysis", *Journal of the American Ceramic Society,* **76,** 2707–26 (1993);

[26]S. C. York, M. W. Abee, D. F. Cox, " -Cr_2O_3 (1012): surface characterization and oxygen adsorption", *Surface Science*, **437**, 386-96 (1999)

[27]E. Lopez-Navarrete, A. R. Gonzalez-Elipe, M. Ocaña, "Non-conventional synthesis of Cr-doped SnO_2 pigments", *Ceramics International,* **29**, 385-392 (2003)

[28]SR. D. Shannon, "Revised effective ionic radii and systematic studies of interatomic distances in halogenides and chalcogenides", *Acta Crystallographica*, **A32**, 751-67 (1976)

[29]V. Di Castro V, G. Polzonetti, "XPS study of MnO oxidation", *Journal of Electron Spectroscopy and Related Phenomena,* **48,** 117-23 (1989)

[30]V. M. Jiménez, A. Fernández, J. P. Espinós, A. R. González-Elipe, "The state of the oxygen at the surface of polycrystalline cobalt oxide", *Journal of Electron Spectroscopy and Related Phenomena,* **71,** 61 (1995)

[31]F. Matteucci F, G. Cruciani, M. Dondi, M. Raimondo, "The Role of Counterions (Mo, Nb, Sb, W) in Cr-, Mn-, Ni- and V-doped Rutile Ceramic Pigments. Part 1. Crystal Structure and Phase Transformations", *Ceramics International*, **32**, 385-92 (2006)

[32]M. Dondi, G. Cruciani, G. Guarini, F. Matteucci, M. Raimondo, "The Role of Counterions (Mo, Nb, Sb, W) in Cr-, Mn-, Ni- and V-doped Rutile Ceramic Pigments. Part 2. Colour and Technological Properties", *Ceramics International*, **32**, 393-405 (2006)

[33]K. Ikeda, H. Schneider, M. Akasaka, H. Rager, "Crystal-field spectroscopic study of Cr-doped mullite", *American Mineralogist,* **77,** 251-7 (1992)

[34]M. Czaja, Z. Mazurak, M. Godlewski, A. Suchocki, "Crystal-field analysis of the Cr^{3+} at monoclinic symmetry (Cs) in $Ca_2Al_3Si_3O_{12}(OH)$ zoisite from Tanzania", *Journal of Applied Spectroscopy*, **62,** 643-7 (1995)

[35]E. Grey, C. Li, T. Ness, "Nonstoichiometric Li-Pseudobrookite(ss) in the $Li_2O-Fe_2O_3-TiO_2$ system", *Journal of Solid State Chemistry,* **141,** 221-8 (1998)

[36]W. D. Carlson, G. R. Rossman, "Vanadium- and chromium-bearing andalusite: occurrence and optical absorption spectroscopy", *American Mineralogist*, **73**,1366-9 (1988)

[37]K. Ullrich, O. Ott, K. Langer, K.D. Becker, "Temperature dependence of the polarized electronic absorption spectra of olivines. Part II-Cobalt-containing olivines", *Physics and Chemistry of Minerals* **31**: 247-602004;

[38]M. Llusar M, A. Fores, J. A. Badenés, J. Calbo, M. A. Tena, G. Monros, "Colour analysis of some cobalt-based blue pigments", *Journal of the European Ceramic Society,* **21,** 1121-30 (2001)

[39]A. Fores A, M. Llusar, J. A.Badenés, J. Calbo, M. A. Tena, G. Monros, "Cobalt minimisation in willemite ($Co_xZn_{2-x}SiO_4$) ceramic pigments", *Green Chemistry* **2,** 93-100 (2000)

[40]T. C. Brunold, H. U: Gudel, E. Cavalli, "Absorption and luminescence spectroscopy of Zn_2SiO_4 willemite crystals doped with Co^{2+}", *Chemical Physics Letters* **252,** 112-20 (1996)

[41]R. A. Eppler, "Colorants for ceramics"; p. 877–92, in. Encyclopedia of chemical technology, Vol. 8, Edited by R.E. Kirk and D.F. Othmer, Wiley, New York, 1998

Table I

Composition of the doped-tialite samples

Sample name	Tialite stoichiometry	Ti/Al	Cr/Tialite mol ratio	Mn/Tialite mol ratio	Co/Tialite mol ratio	Mg/Al
Cr5	Al_2TiO_5	0.5	0.05			
Cr10	Al_2TiO_5	0.5	0.10			
Cr14	Al_2TiO_5	0.5	0.14			
Cr20	Al_2TiO_5	0.5	0.20			
Mn5	Al_2TiO_5	0.5		0.05		
Mn8	Al_2TiO_5	0.5		0.08		
Mn11	Al_2TiO_5	0.5		0.11		
Mn14	Al_2TiO_5	0.5		0.14		
Co5	Al_2TiO_5	0.5			0.05	
Co8	Al_2TiO_5	0.5			0.08	
Co11	Al_2TiO_5	0.5			0.11	
MgMn5	$Al_{1.8}Ti_{1.1}Mg_{0.1}O_5$	0.61		0.05		0.055
MgCo5	$Al_{1.8}Ti_{1.1}Mg_{0.1}O_5$	0.61			0.05	

Table II
Unit cell parameters and unit cell volume of the doped-tialite samples fired at 1400ºC

Sample	a (Å)	b (Å)	c (Å)	V(Å^3)
Undoped tialite	9.4348± 0.0004	9.6424± 0.0004	3.5942 ±0.0002	326.98± 0.04
Cr5	9.4359± 0.0003	9.6421± 0.0004	3.5974± 0.0002	327.30 ± 0.04
Cr10	9.4407± 0.0012	9.6416± 0.0010	3.6048± 0.0004	328.12 ± 0.11
Cr14	9.4443± 0.0003	9.6411± 0.0003	3.6099± 0.0001	328.69 ± 0.03
Cr20	9.4468± 0.0005	9.6404± 0.0004	3.6157± 0.0002	329.28 ± 0.05
Mn5	9.4456± 0.0009	9.6571± 0.0009	3.5974± 0.0004	328.14 ± 0.10
Mn8	9.4522± 0.0008	9.6632± 0.0008	3.6004± 0.0003	328.85 ± 0.08
Mn11	9.4557± 0.0011	9.6682± 0.0012	3.6033± 0.0005	329.41 ± 0.12
Mn14	9.4618± 0.0005	9.6740± 0.0006	3.6042± 0.0002	329.90 ± 0.07
Co5	9.4535± 0.0007	9.6645± 0.0007	3.5991 ±0.0003	328.83 ± 0.07
Co8	9.4637± 0.0010	9.6782± 0.0011	3.6021 ±0.0005	329.92 ± 0.12
Co11	9.4673± 0.0012	9.6823± 0.0014	3.5997 ±0.0005	329.97 ± 0.13
Mg-doped tialite	9.4685± 0.0004	9.6794 ± 0.0004	3.6059± 0.0002	330.48 ± 0.03
Mg/Mn5	9.4805± 0.0006	9.6950 ± 0.0006	3.6098± 0.0003	331.79 ± 0.07
Mg/Co5	9.4790± 0.0007	9.6935 ± 0.0007	3.6051± 0.0003	331.25 ± 0.08

Table III
L*a*b* parameters and colour measured for the doped-tialite pigments fired at 1400ºC and for the glazes

Sample	L* Pigment/Glaze	a*(g-r) Pigment/Glaze	b* (b-y) Pigment/Glaze	Colour Pigment/Glaze
Cr5	70.9	-8.8	13.1	Green
Cr10	69.8	-8.3	13.2	Green
Cr14	65.7/51.0	-9.4/-1.6	15.2/25.8	Green/green
Cr20	63.5	-9.1	15.0	Green
Mn5	49.4/57.0	9.4/11.7	11.5/17.7	Brown/brown
Mn8	45.3	8.2	6.0	Brown
Mn11	42.4	6.2	6.0	Dark brown
Mn14	42.0/52.8	5.2/10.0	4.3/13.0	Dark Brown/brown
Co5	65.7/60.7	4.0/-1.5	13.8/3.3	Light salmon pink/grey
Co8	58.3	2.6	11.8	Beige
Co11	53.7	-1.2	6.3	Beige
MgMn5	50.6/60.9	10.1/10.6	12.0/17.8	Brown/brown
MgCo1	58.0/61.0	0.1/-0.9	9.2/8.3	Beige /grey

Table IV
Energy and splitting of bands of sixfold-coordinated Cr(III) (sample Cr14) and Co(II) (sample Co5)

Cr(III) transitions ($^4A_{2g}\rightarrow$)	Calculated energy (cm^{-1})	Experimental energy (cm^{-1})	Band splitting FWHM (cm^{-1})
$^4T_{2g}$	15210	15240	4660
$^4T_{1g}$	21870	21990	5200
^2E_g	12010	12940	-
$^2T_{1g}$	14080	14570	-
$^2T_{2g}$	19200	19160	-
Co(II) transitions $^4T_{1g}$ (^4F) $\rightarrow$	Calculated energy (cm^{-1})	Experimental energy (cm^{-1})	FWHM (cm^{-1})
$^4T_{2g}$	8890	9220	1970
$^2T_{2g}$	13760	15180	2950
$^4A_{2g}$	17780	17440	1610
$^4T_{1g}$ (^4P)	18810	18780	1430
$^2A_{1g}$	21720	20030	1440

Table V
Energy (cm^{-1}) of Mn(III) bands, orbital baricentres, and crystal field strength calculated as difference between the ^5E_g and $^5T_{2g}$ orbitals

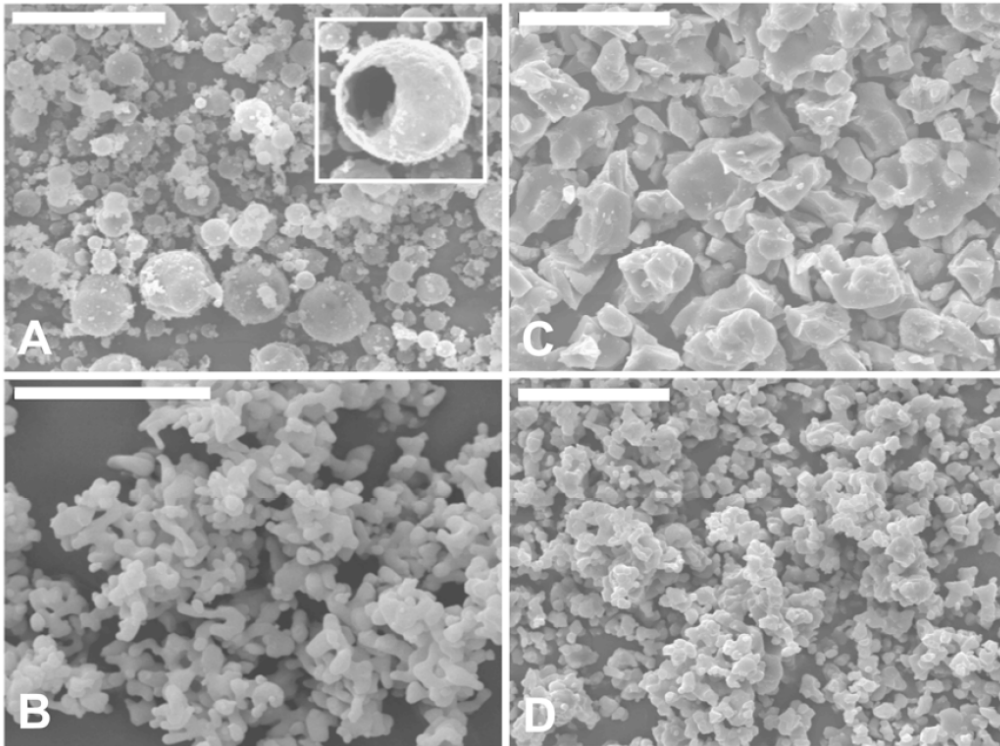| Orbital			Mn5	MgMn5	Mn14
^5E_g	e_g	$^5B_{1g}$	Ground state		
		$^5A_{1g}$	10930	11150	11210
$^5T_{2g}$	t_{2g}	^5E_g	19090	19310	19210
			22770	22520	22650
Baricentre of ^5E_g orbitals			5465	5575	5605
Baricentre of $^5T_{2g}$ orbitals			20930	20915	20930
Crystal field strength (10Dq)			15465	15340	15325

Fig. 1. Scanning electron micrographs obtained for: A) sample Cr5, as prepared (a magnified view of a single particle is shown in the inset for a better observation of its hollow nature; B) sample Cr5 calcined at 1400ºC; C) sample Mn5 calcined at 1400ºC; D) sample Co5 calcined at 1400ºC. Magnification bar = 20　m
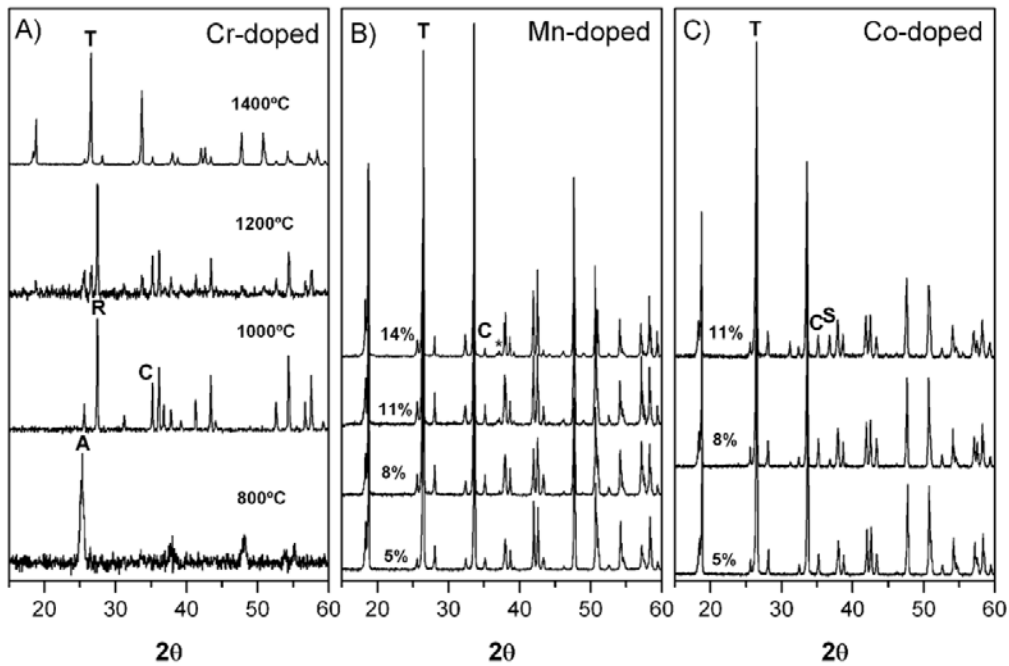

Fig. 2. X-ray diffraction patterns of: A) sample Cr5 heated at different temperatures; B) Mn-doped samples with different Mn content heated at 1400ºC; C) Co-doped samples with different Co content heated at 1400ºC. Symbols designating the most intense reflections of phases: T = tialite, R = TiO_2 rutile, A = TiO_2 anatase, C = Al_2O_3 corundum, S = $CoAl_2O_4$ spinel. Peak marked with an asterisk could not be identified.

13
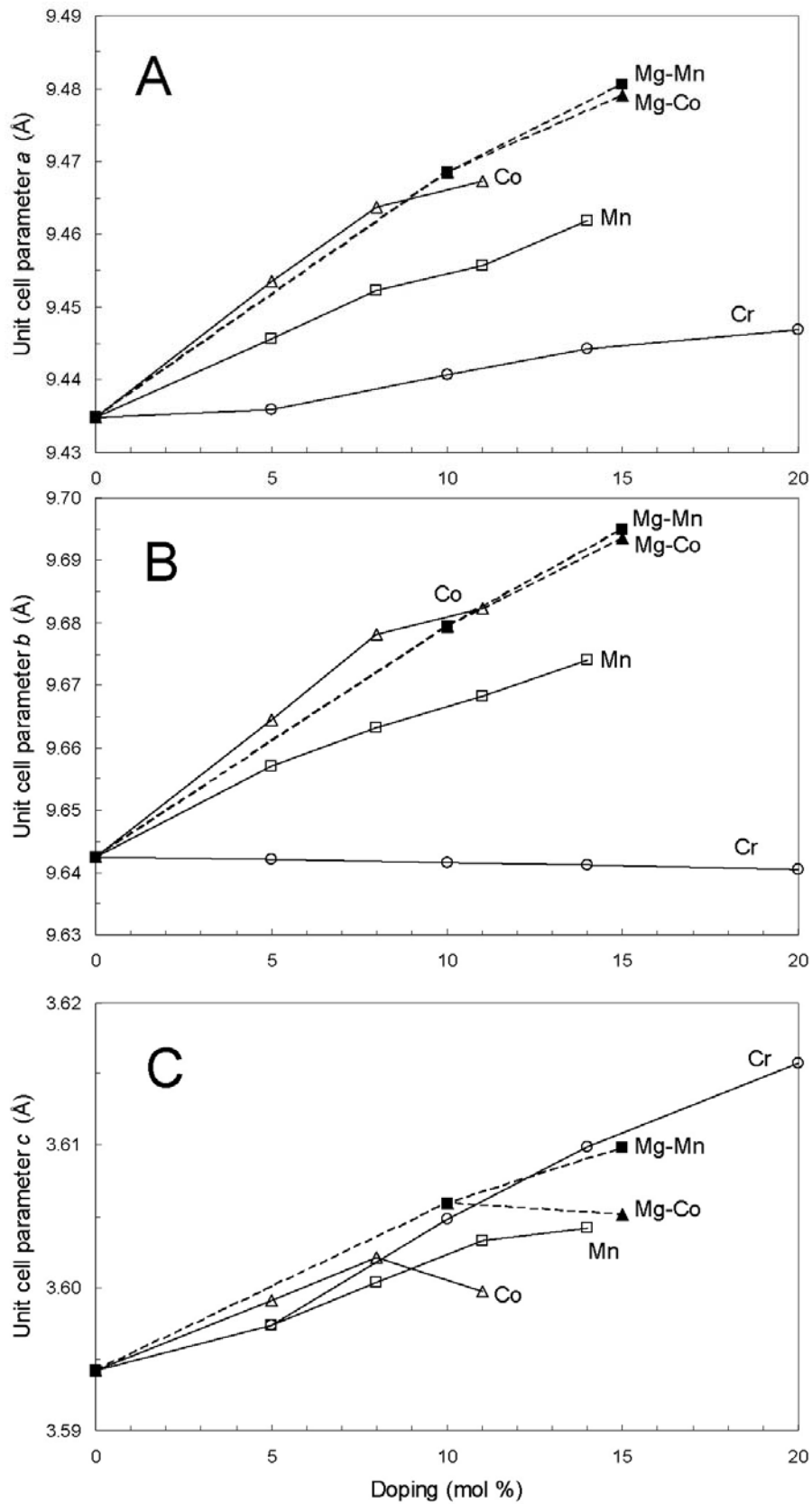
Fig. 3. Changes of unit cell parameters of tialite samples heated at 1400ºC with increasing Co, Cr, or Mn doping and with Mg-Co or Mg-Mn co-doping.

Cr^{3+} c +0.11

b -0.01   a +0.06

Mn^{3+} c +0.07

a +0.19

b +0.23
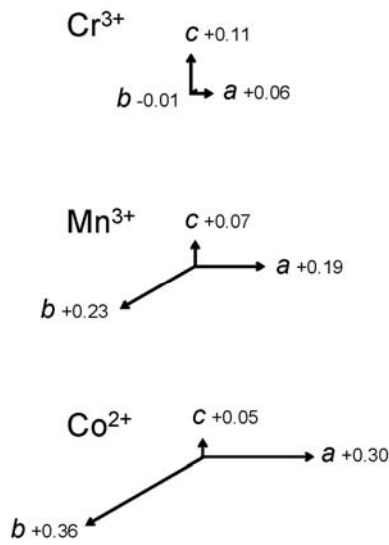
Co^{2+} c +0.05

a +0.30

b +0.36

Fig. 4. Trends of unit cell parameters of tialite pigments with doping (pm per mole of dopant).
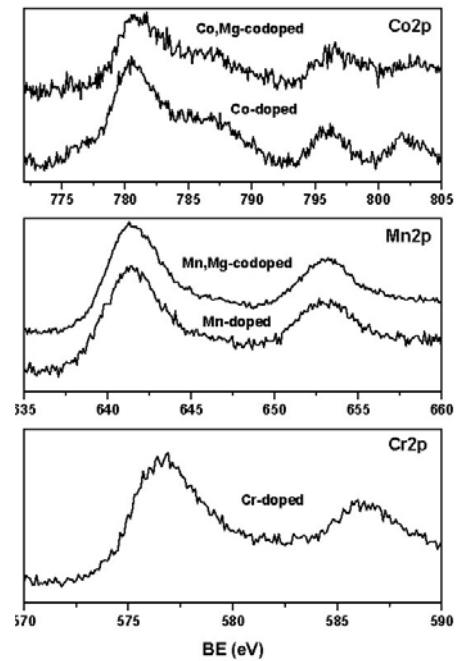
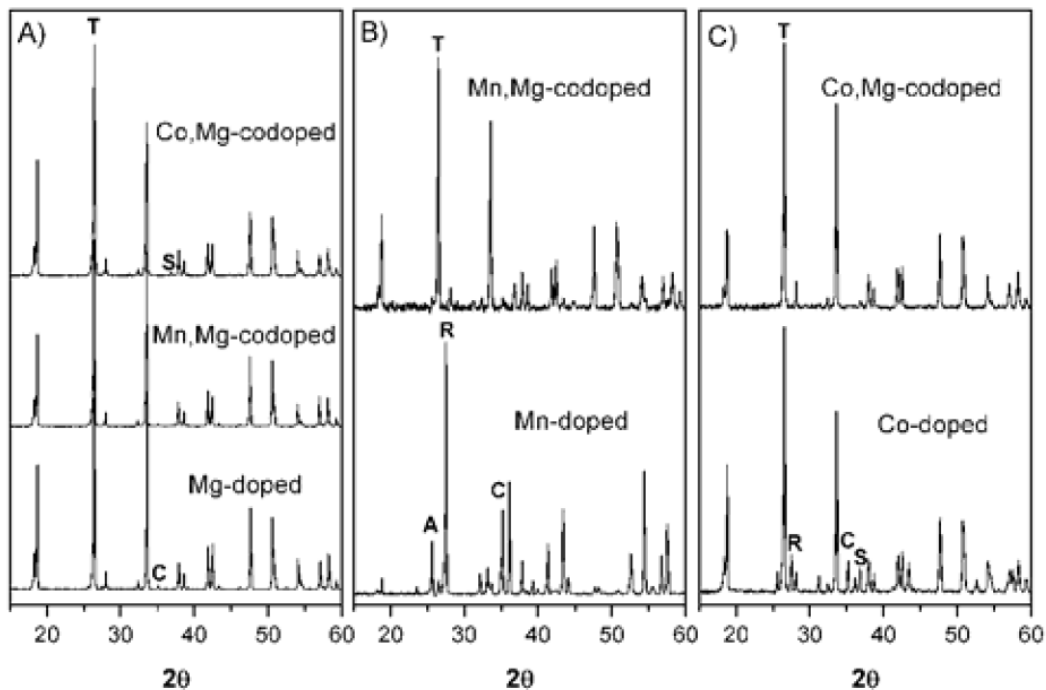Fig. 5. XPS spectra recorded for the Cr-doped, Mn-doped, Mn+Mg codoped, Co-doped and Co+Mg codoped tialite samples heated at 1400ºC.

Fig. 6. X-ray diffraction patterns of: A) Mg-doped, Mn+Mg codoped and Co+Mg codoped tialite samples heated at 1400ºC; B) Mn-doped and Mn+Mg codoped samples after a second firing treatment at 900ºC for 20 h; C) Co-doped and Co+Mg codoped samples after a second firing treatment at 900ºC for 20 h. Symbols designating the most intense reflections of phases: T = tialite, R = TiO_2 rutile, A = TiO_2 anatase, C = Al_2O_3 corundum, S = $CoAl_2O_4$ spinel
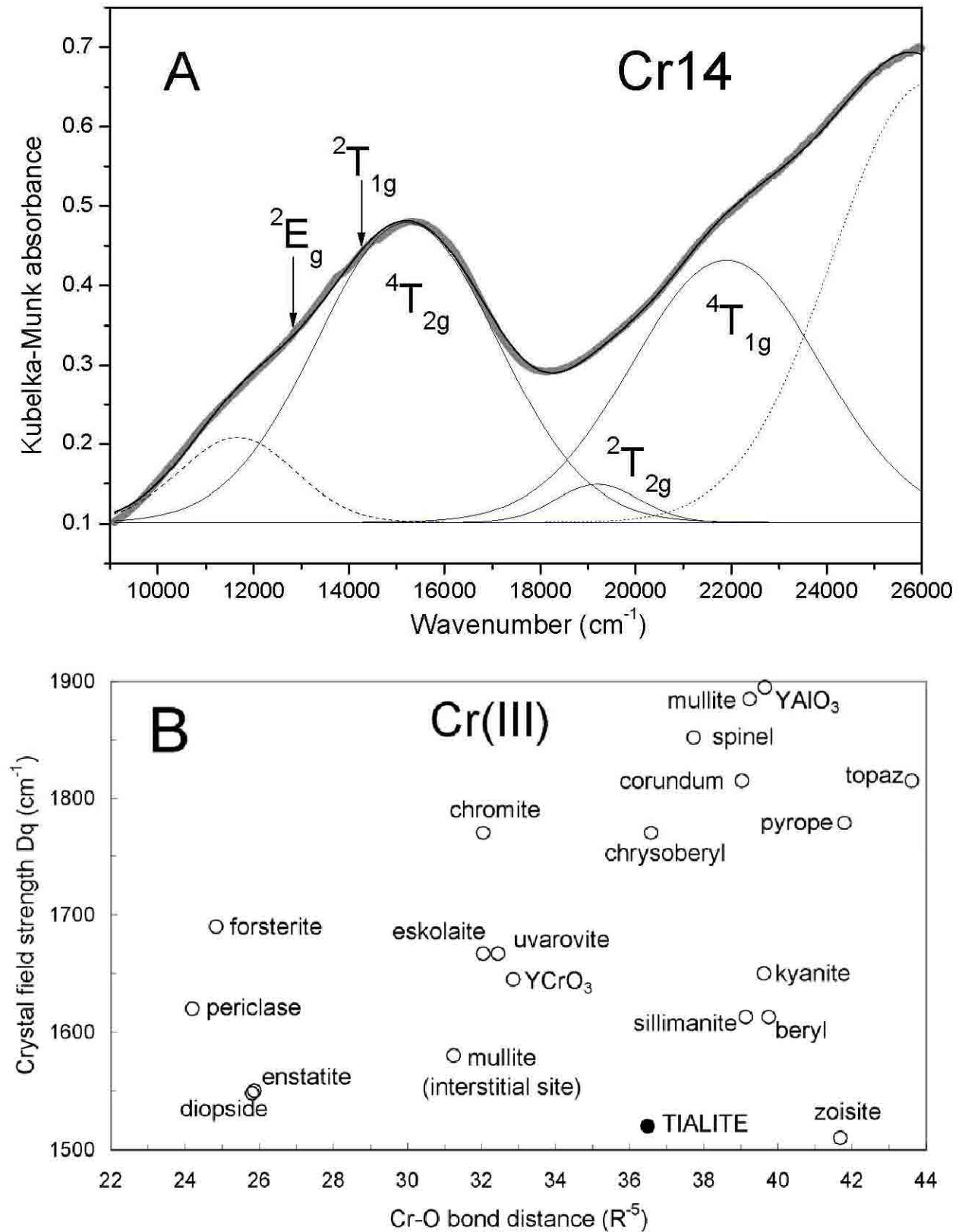
15

Fig. 7. Optical spectrum of the sample Cr14 heated at 1400°C deconvoluted in the bands of octahedrally-coordinated Cr(III) (A) and relationship between Cr-O bond distance and crystal field strength for tialite compared with several oxides and silicates (B).
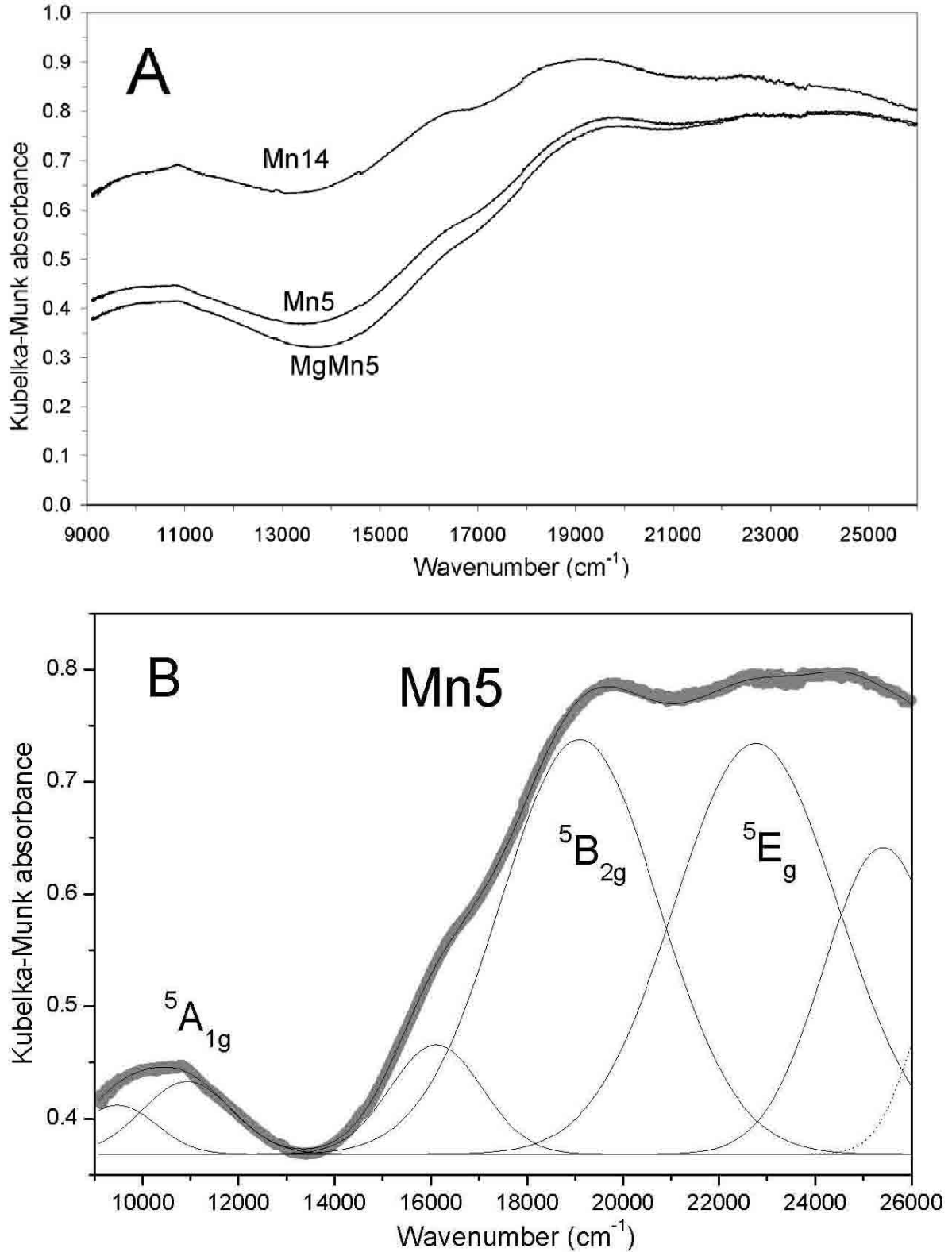
Fig. 8. Optical spectra of manganese-doped tialite samples heated at 1400ºC (A) and deconvoluted spectrum of the sample Mn5 with the bands of Mn(III) in six-fold coordination (B).
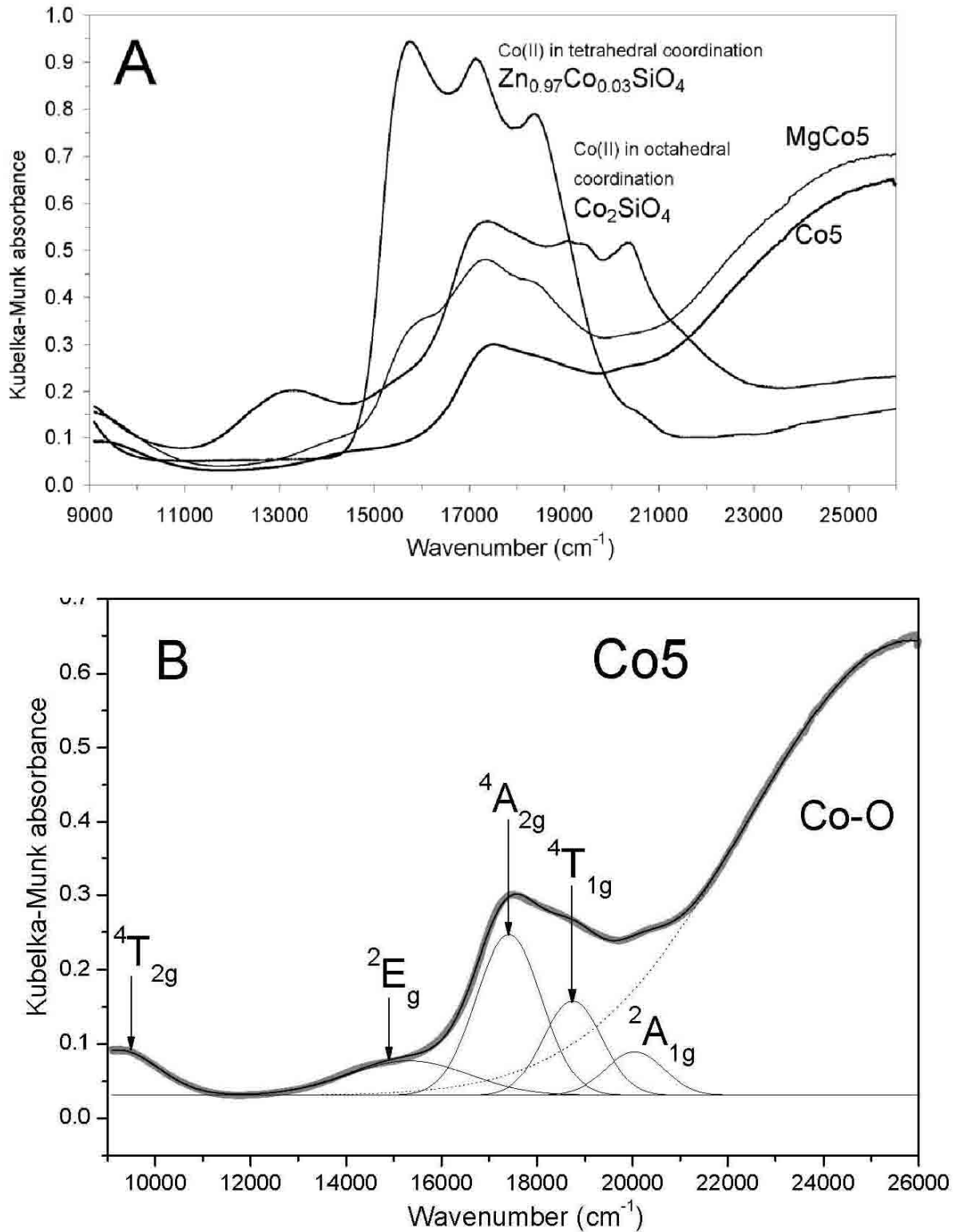
Fig. 9. Optical spectra of tialite samples doped with cobalt (Co5) and co-doped with Mg+Co (MgCo5) and heated at 1400ºC, compared with spectra of octahedrally-coordinated Co(II) in olivine and tetrahedrally-coordinated Co(II) in willemite (A); deconvoluted spectrum of sample Co5 with the bands of Co(II) in six-fold coordination (B).

Fig. 10. Ceramic glazes prepared with Cr-doped (Cr14) Mn-doped (Mn5) and Co-doped (Co5) tialite pigments.